

End-to-End Autonomous Driving through V2X Cooperation

Haibao Yu^{1,2*}, Wenxian Yang^{2*}, Jiaru Zhong^{2,3*}, Zhenwei Yang^{2,4},
Siqi Fan², Ping Luo¹, and Zaiqing Nie^{2†}

¹ HKU ² AIR, Tsinghua University ³ Beijing Institute of Technology
⁴ University of Science and Technology Beijing

Abstract. Cooperatively utilizing both ego-vehicle and infrastructure sensor data via V2X communication has emerged as a promising approach for advanced autonomous driving. However, current research mainly focuses on improving individual modules, rather than taking end-to-end learning to optimize final planning performance, resulting in underutilized data potential. In this paper, we introduce UniV2X, a pioneering cooperative autonomous driving framework that seamlessly integrates all key driving modules across diverse views into a unified network. We propose a sparse-dense hybrid data transmission and fusion mechanism for effective vehicle-infrastructure cooperation, offering three advantages: 1) Effective for simultaneously enhancing agent perception, online mapping, and occupancy prediction, ultimately improving planning performance. 2) Transmission-friendly for practical and limited communication conditions. 3) Reliable data fusion with interpretability of this hybrid data. We implement UniV2X, as well as reproducing several benchmark methods, on the challenging DAIR-V2X, the real-world cooperative driving dataset. Experimental results demonstrate the effectiveness of UniV2X in significantly enhancing planning performance, as well as all intermediate output performance. Code is at <https://github.com/AIR-THU/UniV2X>.

Keywords: End-to-End · Autonomous Driving · V2X

1 Introduction

Despite significant progress achieved through the integration of deep learning, single-vehicle autonomous driving still faces great safety challenges due to limited perceptual range and inadequate information, especially for vehicles relying on cost-effective cameras. Leveraging external sensors, particularly infrastructure sensors with a broader perception field, has shown promising potential for advancing autonomous driving capacities through

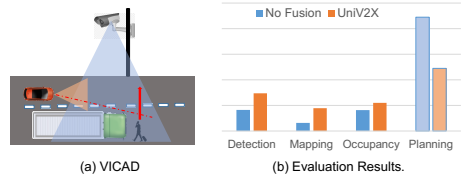


Fig. 1: (a) VICAD: Infrastructure sensor installed highly has broad perception field [14, 57–60, 63], which can supplement the blind and long-range spots of single vehicle. (b) Performance Enhancement: Compared with No Fusion solution, UniV2X achieves significant gains in various tasks, such as detection (+13%), mapping (+11.4%), occupancy prediction (+5.7%), and collision rate (-0.4%).

Table 1: Comparison with the existing methods for cooperative autonomous driving. "AgentP" denotes dynamic object perception. "Map" denotes online mapping. "Occ" denotes occupancy prediction. "-" denotes that the information is not provided or temporarily unable to verify. UniV2X targets planning output and conducts all essential tasks, and the transmitted data is effective, transmission-friendly, and reliable.

Approach	Sensor Data	Transmission				Task				End-to-End
		Type	Effective	Friendly	Reliable	AgentP	Map	Occ	Plan/Control	
V2VNet [47]	Point Cloud	BEV Feature	-	Medium	No	✓				No
CoCa3D [18]	Image	BEV Feature	-	Medium	No	✓				No
CoBEVT [51]	Image	BEV Feature	-	Medium	No	✓	✓			No
PP-VIC [63]	Point Cloud	Detected Result	-	High	Yes	✓				No
DeepA [46]	Image	BEV Feature	-	Medium	No	✓	✓			No
TransIFF [6]	Point Cloud	Instance Feature	-	High	Yes	✓				No
Where2Comm [17]	Point Cloud	Instance Feature	-	High	Yes	✓				No
CSA [45]	Image	Raw Image	Yes	Low	Yes				✓	Non-Explicit
COOPN [9]	Point Cloud	BEV Feature	Yes	Medium	No				✓	Non-Explicit
UniV2X (Ours)	Image	Hybrid Feature	Yes	High	Yes	✓	✓	✓	✓	Explicit

Vehicle-to-Everything (V2X) communication. Several research studies have investigated the efficacy of external sensor data in diverse tasks such as detection [18, 35, 44, 47, 61], tracking [63], segmentation [51], localization [10, 20], and forecasting [36, 40, 63]. However, existing solutions primarily emphasize individual task optimization, neglecting the overall planning enhancement. This creates challenges in comprehensive data exploitation, driven by a misalignment between individual task goals and final planning objectives. Thus, end-to-end learning exploration, which directly optimizes the final planning output by harnessing both onboard and external sensor data, becomes necessary. In this paper, we focus on vehicle-infrastructure cooperative autonomous driving (VICAD), with images as input data. We also consider verifying UniV2X on V2V scenes.

The VICAD problem can be formulated as a planning-centric optimization with multiple-view sensor inputs under constrained communication bandwidth. Compared with single-vehicle autonomous driving, VICAD poses additional challenges when addressed through end-to-end learning. Firstly, the transmitted infrastructure data must enhance both critical modules and the final planning performance in autonomous driving. These critical modules encompass dynamic obstacle perception, online mapping, and grid occupancy-based general obstacle detection, providing an explicit scene representation crucial for ensuring the safety of autonomous driving. Second, driven by real-time requirements and limited communication conditions, minimizing transmission costs becomes crucial to mitigate communication bandwidth consumption and reduce latency. Thirdly, transmitted data must be interpretable, allowing the vehicle to verify and judiciously employ the data to prevent potential safety issues such as communication attacks and data corruption. Addressing these challenges necessitates a well-designed solution for data transmission and cross-view data fusion.

Here are a few straightforward attempts to address the cooperative driving problem through end-to-end learning. CSA [45] directly shares and feeds raw images received from other vehicles into basic neural networks for control output. CooperNaut [9] shares features derived from point clouds among vehicles and inputs them into a basic CNN network for the final output. However, these existing solutions rely on a vanilla approach, utilizing simple networks to optimize plan-

ning and control outputs. This paradigm lacks explicit modules, compromising safety assurance and interpretability. Especially within intricate urban settings, this approach falls short in ensuring the reliability of the driving system.

To this end, we introduce UniV2X, an innovative cooperative autonomous driving framework that seamlessly integrates pivotal modules and cross views into a unified network, as depicted in Figure 2. Beyond the final planning task, we address three common tasks for scene representation in autonomous driving: 1) agent perception, encompassing 3D object detection, tracking, and motion forecasting for dynamic obstacle perception, 2) road element (especially lane) detection for online mapping, and 3) grid-occupancy prediction for general obstacle perception. Inspired by UniAD [16], we adopt a query-based architecture to establish connections across nodes, encompassing internal modules within infrastructure and ego-vehicle systems, as well as cross-view interactions. In transmission and cross-view interaction, we classify agent perception and road element detection as instance-level representation and occupancy prediction as scene-level representation. We transmit agent queries and lane queries for cross-view agent perception interaction and online mapping interaction. We transmit the occupied probability map, recognizing its dense nature at the scene-level occupancy, for cross-view occupancy interaction. This transmission, termed sparse-dense hybrid transmission, balances sparsity and density in spatial and feature dimensions, respectively. Cross-view data fusion, such as agent fusion, mainly involves temporal and spatial synchronization, cross-view data matching and fusion, data adaptation for planning and intermediate outputs. The resulting lightweight approach strengthens dynamic object perception, online mapping, and occupancy modules, thereby enhancing planning performance. Moreover, the interpretability of queries and occupied probability maps at the instance and scene levels, respectively, fortifies the reliability of the VICAD system, bolstering its transmission integrity and fusion safety.

The contributions are summarized as follows:

- We pioneer a first explicitly end-to-end framework that unifies vital modules within a single model, advancing the landscape of cooperative autonomous driving. Notably, UniV2X is the first end-to-end framework for VICAD.
- We design a sparse-dense hybrid transmission and cross-view data interaction approach, aligning with effectiveness, transmission-friendliness, and reliability prerequisites for end-to-end cooperative autonomous driving.
- We reproduce several cooperative methods as benchmarks, as well as instantiating the UniV2X framework on DAIR-V2X [60] and V2X-Sim [25]. Experimental results underscore the efficacy of our end-to-end paradigm.

2 Related Works

Cooperative Autonomous Driving. Leveraging V2X communication for cooperative autonomous driving has garnered significant attention. Works like [5, 18, 26, 31, 42, 47, 54] emphasize transmitting Bird’s Eye View (BEV) features extracted from point clouds or images to improve 3D object detection. [51] employs sparse transformers to enhance segmentation performance, while [36] focuses on utilizing sequential trajectories for motion forecasting. Addressing the latency

issue in cooperation detection, [24, 39, 56, 62] utilize historical frames or features. Additionally, [6, 12, 17] transmit instance-level features or queries to reduce transmission costs and alleviate communication challenges. Datasets for cooperative object perception are provided by [8, 25, 33, 52, 53, 60, 63]. [63] releases a real-world trajectory dataset generated from infrastructure and vehicle sensor data. While most of these works concentrate on single tasks, a few also focus on end-to-end output planning or control tasks. For instance, [45] employs multi-vehicle images with a simple convolutional network to generate control outputs. Similarly, [9] adopts a simple MLP to learn planning outputs with BEV features from multi-vehicle point clouds. However, these solutions lack explicit interpretability modules. In this paper, we present UniV2X, a comprehensive framework that integrates all essential modules within a single model, utilizing end-to-end learning for optimizing final planning improvement as well as intermediate outputs.

End-to-End Autonomous Driving. End-to-end autonomous driving involves the extraction of planning output directly from raw data in a differentiable and learnable manner. Pioneering work, such as [2], employs CNNs to generate control outputs from point cloud data. Others, exemplified by [37, 65], utilize point clouds and High-definition Maps as inputs. Concurrently, works like [38] leverage multi-modal sensor data as input to generate object density maps for visualization. For acquiring driving skills, [7, 34, 50] employ imitation learning (IL) to learn from expert demonstrations in an open-loop manner. In contrast, [19, 21, 30] utilize reinforcement learning (RL) to iteratively learn driving skills by interacting with the environment in a closed-loop fashion. Among related works, UniAD [16] is the first to use queries to connect all essential tasks such as perception, mapping, prediction, and planning. Through unifying these tasks into a single network and employing imitation learning, UniAD achieves remarkable performance on the nuScenes dataset [3]. However, UniAD solely considers single-vehicle sensor data, while our approach, UniV2X, leverages sensor data from diverse views.

3 Method

In this section, we introduce UniV2X, all-in-one solution for vehicle and infrastructure cooperative autonomous driving (VICAD), together with the proposed sparse-dense hybrid data transmission and fusion design, as shown in Figure 2. We start by presenting the VICAD problem and introduce background. Following that, we describe how to generate sparse-dense hybrid data for transmission and cross-view data fusion. The training process is also outlined in this section.

3.1 VICAD Problem Formulation

The VICAD problem is planning-oriented, aiming to improve the planning performance by utilizing both infrastructure sensor data and ego-vehicle sensor data thorough V2X communication. This paper focuses on the images as inputs. The input of VICAD consists of two parts: (a) Ego-vehicle images $\{I_v(t)|t \leq t_v\}$ and the relative pose $M_v(t_v)$ at the current vehicle timestamp t_v . (b) Infrastructure images $\{I_i(t)|t \leq t_i\}$ and the relative pose $M_i(t_i)$ at the current infrastructure

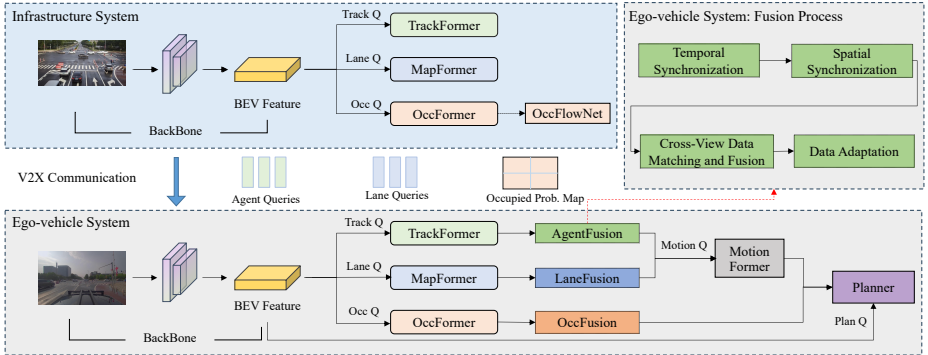


Fig. 2: Pipeline of Unified Autonomous Driving through V2X Cooperation (UniV2X). UniV2X aims to connect and jointly optimize all essential modules across diverse views for enhanced planning performance. Cross-view data interaction bolsters pivotal components in autonomous driving like agent perception, online mapping, and occupancy prediction. Additional flow prediction enables minimizing transmission cost for transmitting occupied probability map. Cross-view data fusion involves temporal and spatial synchronization, cross-view data matching and fusion, and data adaptation.

timestamp t_i . Note that in practical scenario, the timestamp t_i should be earlier than timestamp t_v due to the communication latency. The output of VICAD is to predict future coordinates of ego vehicle for time steps $t = t_v + 1, \dots, t_{pred}$.

Evaluation Metrics. We evaluate the planning performance with L2 Error and Collision Rate, and measure transmission cost with Bytes Per Second (BPS), as suggested in [60, 63]. We provide the detailed explanations in the Appendix.

Challenges. Compared with single-vehicle autonomous driving, VICAD presents additional challenges: (1) Limited by practical communication conditions, fewer infrastructure data should be transmitted to vehicle to minimize bandwidth usage and reduce latency. (2) Wireless communication introduce unavoidable latency, potentially leading to temporal misalignment in data fusion. (3) Potential communication attacks and data corruption can render transmitted data untrustworthy. This highlights the need for interpretable transmitted data.

3.2 Background

Explicit Scene Representation. Planning and decision-making built on explicit scene representation facilitates explainable and trustworthy autonomous driving. Here are several common and vital modules in autonomous driving.

- Agent perception is used for accurately sensing dynamic obstacles (3D Object Detection), correlating obstacles (Tracking), and ultimately predicting their future behavior (Motion Forecasting). Accurate sensing and prediction help avoid collisions and ensure driving safety.
- Online mapping aims at extracting road elements to construct a map in real time, which can be used for positioning and making decisions more compliant with traffic rules like Tesla way [41]. It is considered to be an effective alternative to HD (high-precision) maps, especially for low-cost solutions.

- Grid-based occupancy prediction is used for general obstacle detection by predicting the occupancy of each grid [43, 48]. This is regarded as the effective solution for long-tailed challenges in autonomous driving.

Data for Transmission. It involves three primary types in V2X cooperation:

- Raw data like raw images. This data type maintains all valuable information but requires significant transmission costs.
- Perception outputs like detection results. While communication-friendly, this data is not suitable for seamless integration into an end-to-end framework.
- Intermediate-level data such as Bird’s Eye View (BEV) features and queries [6, 12]. Compared to the above two data, this data achieves a balance between preserving valuable information and reducing redundant transmission.

To ensure effective, transmission-friendly, and reliable transmitted data, we propose a sparse-dense hybrid transmission mechanism. Queries, as lightweight instance-level features, enhance agent perception and online mapping, as dynamic obstacles and lanes can be treated as instance-level representations. Occupied probability maps, channel-sparse scene-level features, improve occupancy prediction. Compared to less interpretable and high-cost BEV features, occupied probability maps offer pixel-level interpretability and lower transmission costs.

3.3 Sparse-Dense Hybrid Data Generation

This part illustrates how to generate sparse-dense hybrid data for transmission in infrastructure system. As depicted in Figure 2, the infrastructure system is composed of: Backbone, TrackFormer, MapFormer, OccFormer, and OccFlowNet.

BEVFormer [27] is adopted as the backbone to extract image features and transform them into bird’s-eye-view (BEV) features B_{inf} with size of (200, 200, 256) by incorporating spatial cross-attention and temporal self-attention. TrackFormer is based on DETR [4], which optimizes detection and multi-object tracking together, eliminating the need for non-differentiable post-processing like NMS [1]. The ultimate filtered output from TrackFormer contains N_a^{inf} valid agent queries $\{Q_A^{inf}\}$ with a feature dimension of 256 and their corresponding assigned tracking IDs and reference points. MapFormer is based on Panoptic SegFormer [28]. We mainly focus on the lane line and crosswalk elements. During transmission, we filter out low-scoring queries using boxes generated from the classification decoder, and exclusively transmit N_l^{inf} valid lane queries $\{Q_L^{inf}\}$ with a feature dimension of 256, along with their corresponding reference points. Original OccFormer in UniAD [16] solely considers instance-level occupancy associated with agent queries, predicting multiple steps. However, occupancy serves as a complementary factor to object perception for general obstacle detection, and transmitting multiple probability maps incurs significant transmission costs. To address these challenges, we retain the dense feature obtained through pixel-level attention with a size of (200, 200, 256). Initially, a Multi-layer Perception (MLP) is employed to transform the dense feature into BEV occupied probability map denoted as P^{inf} with a size of (200, 200). Subsequently, adopting the

feature flow prediction approach [62, 63], an additional probability flow module is utilized to represent T-step maps via a linear operation as

$$P_{future}(t) = P_0 + t * P_1, \quad (1)$$

where P_0 signifies the present BEV probability map, and P_1 indicates the corresponding BEV probability flow. Transmitting T-step occupied probability maps requires $T*200*200$ floats, while UniV2X only requires $2*200*200$ floats.

Advantages of Sparse-Dense Hybrid Data Transmission. Agent queries and lane queries, as instance-level features, exhibit remarkable sparsity in the spatial dimension. Conversely, the BEV occupied probability map is dense in the spatial dimension but is characterized by a single dimension in terms of feature dimension. The probability flow mirrors the sparse-dense characteristics of their respective counterparts, the probability map. Hence, the sparse-dense hybrid data transmission incurs minimal transmission costs and is communication-friendly. A transmission cost comparison is also presented in Table 2.

Table 2: Transmission Cost in Each Transmission. Compared with raw images and BEV feature, hybrid data transmission requires much less transmission cost.

Data Type	Size	Transmission Cost (Bytes)
Raw Image	(1080, 1920, 3)	$\sim 2 \times 10^8$
BEV Feature	(200, 200, 256)	$\sim 4 \times 10^8$
Hybrid Feature	$(N_a^{inf} + N_l^{inf}, 256) \times 2, (200, 200) \times 2$	$\sim 10^5$

3.4 Cross-View Data Fusion (Agent Fusion)

In the ego-vehicle system, the BEV features B_{veh} are first extracted from the images captured by onboard sensors. We also adopt TrackFormer, MapFormer, and OccFormer to generate the corresponding agent queries $\{Q_A^{veh}\}$, lane queries $\{Q_L^{veh}\}$, and the occupied probability map P^{veh} . The network for these modules aligns with that of the infrastructure system. In this section, we describe how to implement cross-view agent fusion. Cross-view agent fusion is mainly composed of temporal synchronization for latency compensation, spatial synchronization to unify the cross-view coordinates, data matching and fusing, and data adaptation for planning and intermediate outputs. Some modules are similar in implementing lane fusion and occupancy fusion.

Temporal Synchronization with Flow Prediction. The transmission delay in wireless communication, as t_i is earlier than t_v , is significant in complex traffic systems, especially for the busy intersection scenario. Due to the movement of dynamic objects, there is a temporal misalignment when fusing data from different sources. To address that, we incorporate feature prediction into infrastructure agent queries to mitigate latency, following feature flow prediction as [62, 63]. Specifically, we input both agent query Q_A^{inf} and query associated in the previous frame into QueryFlowNet, a three-layer Multi-Layer Perceptron (MLP), to generate the agent query flow Q_{AFlow}^{inf} . The dimensions of the agent query flow match those of the agent query. Subsequently, a linear operation

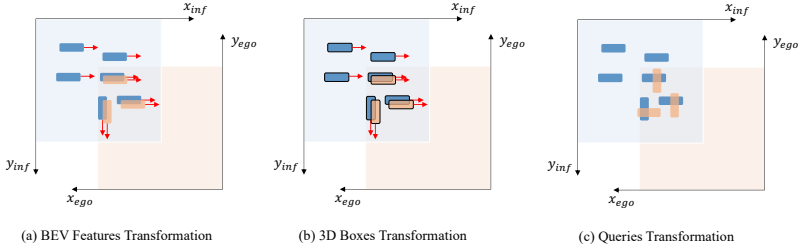


Fig. 3: Object orientation is explicitly encoded in BEV feature maps (a) and bounding box (b), while the orientation is implicitly embedded in the feature of queries (c), resulting in the challenge of cross-view rotation alignment in spatial synchronization.

forecasts future features can be used to mitigate latency $t_v - t_i$, depicted as

$$Q_A^{inf}(t_v) = Q_A^{inf}(t_i) + (t_v - t_i) * Q_{AFlow}^{inf}. \quad (2)$$

Notably, QueryFlowNet of the Flow Prediction module is not trained in an end-to-end manner in UniV2X. We adopt self-supervised learning following [62, 63].

Spatial Synchronization with Rotation-Aware Query Transformation.

We initially transform the reference points of infrastructure agent queries Q_A^{inf} from the infrastructure to the ego-vehicle using the relative pose $[R, T]$ between the infrastructure system and ego-vehicle system. Here, the relative pose is generated from the global relative poses of the two systems, with R representing a rotation matrix and T denoting translation. However, each object inherently possesses 3D information about its location, size, and rotation. In the context of a query representing a 3D object, the location is explicitly denoted by reference points, while the rotation is implicitly encoded within the query’s feature, as illustrated in Figure 3. To address this issue, we propose a solution termed rotation-aware query transformation to achieve spatial synchronization. This involves inputting the infrastructure query, along with its rotation R in the relative pose, into a three-layer MLP to update the feature with rotation awareness, achieving explicit spatial synchronization as

$$\text{spatial_update}(Q_A^{inf}) = \text{MLP}([Q_A^{inf}, R]), \quad (3)$$

where the rotation matrix R is reshaped into 9 dimensions. Finally, we transform the infrastructure agent query data into the ego-vehicle coordinate system.

Cross-View Query Matching and Fusion. At this stage, cross-view agent queries are temporally and spatially synchronized. To match corresponding queries from different sides, we calculate the Euclidean distance of their reference points and employ the Hungarian method [22]. For the matched query pairs Q_A^{inf} and Q_A^{veh} , they are fed into a three-layer MLP to generate the cooperated query Q_A , which is used to update the ego-vehicle agent query Q_A^{veh} . For the unmatched queries from infrastructure, they are utilized to be added to the ego-vehicle queries. Finally, we assign tracking IDs and filter out cross-view fused queries with low detection confidence, resulting in the ultimate agent queries.

Ego Identification and Removing. This module is used to eliminate the problem of false detection in the ego-vehicle area. From the infrastructure view, the ego vehicle can be perceived either as a distinct obstacle in agent perception or as part of the occupied area in occupancy prediction. Following cross-view data fusion, there is a possibility of generating an obstacle query within the region where the ego vehicle is located, thereby marking the ego-vehicle area as occupied. Such an occurrence can significantly disrupt decision-making processes and ultimately impact decision-making performance. To mitigate this issue, we define the ego-vehicle area as a rectangle, filter queries within this area, and designate this region as unoccupied. This configuration proves effective in enhancing planning performance, particularly in the L2 Error evaluation. However, this straightforward solution may not consistently perform optimally due to relative position errors between infrastructure and ego vehicle, stemming from positioning and calibration inaccuracies [13, 55]. Further exploration and refinement are essential to contribute to cooperative autonomous driving.

Decoder Input Augmentation for Intermediate Output. Through cross-attention between ultimately fused agent queries and the output from the encoder in the ego-vehicle TrackFormer, we can obtain intermediate outputs for agents, such as 3D detection outputs, to enhance the interpretability of UniV2X. However, the output of the encoder is all generated from ego-vehicle sensor data information, rendering queries from the infrastructure unable to produce corresponding agent outputs. To address this issue, we use synchronized infrastructure queries to enhance ego-vehicle BEV features, the output of the encoder, as:

$$\text{update}(B^{veh}) = B^{veh} + \text{MLP}(\text{synchronized}(Q_A^{inf})). \quad (4)$$

3.5 Cross-View Data Fusion (Lane Fusion)

The LaneFusion module is utilized to fuse lane queries across different sides. In this context, we omit temporal synchronization in lane fusion, as the road lane elements remain unaffected by latency and maintain stability. Similar to AgentFusion, LaneFusion incorporates spatial synchronization through the rotation-aware query transformation. This process converts infrastructure lane queries, comprising reference points and query features, into the ego-vehicle coordinate system. We then match and fuse the synchronized infrastructure lane queries with ego-vehicle lane queries, as done in AgentFusion. To accelerate training, we also choose to directly concatenate synchronized queries with ego-vehicle lane queries. The synchronized queries are also used for decoder input augmentation.

3.6 Cross-View Data Fusion (Occupancy Fusion)

We first generate multiple-step infrastructure occupied probability maps through linear operations, aligning them with ego-vehicle multiple-step occupancy predictions. Leveraging the explicit representation of rotation in the dense probability map, we directly transform the infrastructure occupied probability maps to the ego-vehicle system using the relative pose. Subsequently, we fuse the synchronized occupied probability maps with ego-vehicle occupied probability maps

using simple max operations, generating the fused probability map \hat{P} . Grids with a probability exceeding a certain threshold are marked as occupied.

3.7 Planning Output

Based on the fused agent queries, lane queries, and occupancy features, we reused the implementations in UniAD [16] to generate final planning output. MotionFormer is used to generate a set of N_a motion queries with a prediction horizon of t_{pred} . These queries are created by capturing the interactions among agents, lanes, and goals. Notably, these agent queries encompass the ego-vehicle query, thereby enabling MotionFormer to generate ego-vehicle queries with multimodal intentions. The BEV occupied probability map \hat{P} is utilized to create a binary occupancy map \hat{O} . In the planning phase, the ego-vehicle query obtained from MotionFormer is combined with command embeddings to shape a "plan query". These commands comprise turning left, turning right, and moving forward. This plan query, along with the BEV feature, is input into the decoder to produce future waypoints. The ultimate planning trajectory is derived by minimizing a cost function, ensuring the avoidance of collisions with occupied grids \hat{O} .

3.8 UniV2X Training

In our work, we train UniV2X with imitation learning. Specifically, to ensure comprehensive and stable training, we adopt a four-stage training strategy. In the first stage, we pre-train the infrastructure system, including tracking, online mapping, and occupancy prediction tasks, with the annotations from infrastructure view as ground truth. In the second stage, we focus on pre-training perception tasks within the ego-vehicle system. This stage encompasses tasks like tracking and online mapping, employing the vehicle-view annotations as ground truth. In the third stage, all fusion modules and all modules in ego-vehicle systems, as well as all tasks, are trained. Cooperative-view annotations are used as the ground truth for this stage, with the following combined losses:

$$L = L_{track} + L_{map} + L_{motion} + L_{occ} + L_{plan}. \quad (5)$$

Furthermore, we use self-supervised learning to train QueryFlowNet and OccFlowNet. This involves constructing infrastructure frame pairs and employing a similarity loss for training, similar to the strategy described in [62].

4 Experiments

In this section, we implement UniV2X, alongside reproducing various perception, online mapping, and end-to-end methods on DAIR-V2X [60, 63]. Experiment results showcase the effectiveness, transmission-friendliness, and reliability of our design. More details, ablation studies and visualizations are provided in the Appendix. Furthermore, we conduct UniV2X on more V2X datasets such as V2X-Sim [25], and present the experiment results in the Appendix.

Table 3: Planning Evaluation Results. We do not report the results at 0.5s and 1.5s because most of the collision rate is zero. UniV2X significantly surpasses all reproduced end-to-end baselines in collision rate, while requiring much less transmission cost.

Method	L2 Error (m)↓				Col. Rate (%)↓				Trans. Cost↓
	2.5s	3.5s	4.5s	Avg.	2.5s	3.5s	4.5s	Avg.	
No Fusion	2.58	3.37	4.36	3.44	0.15	1.04	1.48	0.89	0
Vanilla	2.21	3.31	4.46	3.33	0.15	0.89	2.67	1.24	8.19×10^7
V2VNet [47]	2.31	3.29	4.31	3.30	0.00	1.03	1.47	0.83	8.19×10^7
CooperNaut [9]	3.83	5.26	6.69	5.26	0.59	1.92	1.63	1.38	8.19×10^7
UniV2X (Ours)	2.60	3.34	4.36	3.43	0.00	0.74	0.74	0.49	8.09×10^5

4.1 Experiment Settings

DAIR-V2X Dataset comprises approximately 100 scenes captured at 28 complex traffic intersections, recorded using both infrastructure and vehicle sensors. Each scene has a duration ranging from 10 to 25 seconds, capturing data at a rate of 10 Hz, and is equipped with a high-definition (HD) map. This dataset provides a diverse range of driving behaviors, including actions such as moving forward, turning left, and turning right. To align with nuScenes [3], we categorize object classes into four categories (car, bicycle, pedestrian, traffic_cone).

UniV2X Implementation Details. We establish the interest range of the ego vehicle as $[-50, 50, -50, 50]$ meters. The ego-vehicle BEV range is defined within a rectangular area spanning $[-50, 50, -50, 50]$ meters, with each grid measuring 0.25m by 0.25m. The infrastructure BEV range is set as $[0, 100, -50, 50]$ meters, accounting for the camera’s forward sensing range and facilitating more effective utilization of infrastructure data. The experiments are conducted utilizing 8 NVIDIA A100 GPUs. More implementation details can be found in the appendix.

Baseline Settings. No Fusion only utilizes ego-vehicle images as sensor data input, without any infrastructure data input. In Vanilla approach, we employ a simple CNN to fuse infrastructure and ego-vehicle BEV features. The fused BEV feature is reshaped into one dimension and subsequently fed into a Multi-Layer Perceptron (MLP) to generate the planning path. In V2VNet [47] approach, we use a CNN to fuse two-side BEV features into a new ego-vehicle BEV feature, and send this new feature into UniAD [16]. In CooperNaut [9], we also employ a CNN to fuse two-side BEV features, with only one frame input each time. Given the significant role of ego status, such as ego-vehicle velocity, in open-loop end-to-end autonomous driving, as illustrated in [29], we remove the ego-vehicle velocity embedding in all baseline settings for a fair comparison. Additionally, we explore the role of ego-vehicle velocity for UniV2X in the appendix.

4.2 Experiment Results on DAIR-V2X

Planning Results. We report the planning results in Table 3. Compared with No Fusion, UniV2X achieves a 45% decreasing in average collision rate in Table 3. In particular, as the planning time increases, the performance improvement

becomes more obvious. This result effectively illustrates that the use of infrastructure information can improve autonomous driving performance, especially for low-cost monocular solutions. Compared with Vanilla, V2VNet methods, and CooperNaut, UniV2X behaves much better in average collision rate (0.49 *vs* 1.24, 0.49 *vs* 0.83, 0.49 *vs* 1.38). Note that we ignore the evaluation result comparisons in L2 Error since most methods achieve similar L2 Error results. Furthermore, UniV2X requires much less transmission cost than Vanilla as well as V2VNet and CooperNaut solutions (8.09×10^5 *vs* 8.19×10^7). So that our UniV2X requires much less transmission cost and is more transmission-friendly.

Agent Perception Results. We employ various fusion strategies on DAIR-V2X, including No Fusion (no fusing infrastructure data), Early Fusion (fusing raw infrastructure BEV feature), and Late Fusion (fusing infrastructure detection results with Hungarian method [23]). Additionally, we reproduce current SOTA cooperative perception methods on DAIR-V2X, namely V2X-ViT [52], Where2comm [17], and DiscoNet [26]. For a fair comparison, we standardize inputs (image-only) and evaluation settings. All methods, except for CoCa3D [18] based on depth estimation, are re-implemented using BEVFormer [27].

Table 4: Detection and Multi-Object Tracking Evaluation Results.

Method	mAP \uparrow	AMOTA \uparrow	Trans. Cost (BPS) \downarrow
No Fusion	0.165	0.163	0
Early Fusion	0.243	0.209	8.19×10^7
Late Fusion+AB3DMOT [49]	0.196	0.263	6.60×10^2
CoCa3D [18]	0.226	-	4.63×10^6
V2X-ViT [52]	0.268	0.287	2.56×10^6
Where2comm [17]	0.162	0.106	5.40×10^5
DiscoNet [26]	0.216	0.203	1.60×10^5
V2X-ViT [52]+Where2comm [17]	0.178	0.071	7.22×10^4
UniV2X (Ours)	0.295 (+0.13)	0.239 (+0.076)	6.96×10^4

We present the evaluation results (car class) for detection and tracking in Table 4. (1) UniV2X demonstrates a notable enhancement of **+7.6** and **+3.0** in AMOTA(%) compared to No Fusion and Early Fusion. (2) UniV2X outperforms CoCa3D, Where2comm, and DiscoNet at similar or less transmission cost. (3) While UniV2X follows an end-to-end paradigm, achieving inferior tracking performance compared to tracking-by-detection methods with complex association, such as Late Fusion+AB3DMOT (0.239 *vs* 0.263 at AMOTA), it significantly outperforms this tracking-by-detection solution in detection (0.295 *vs* 0.196). It is important to note that this tracking-by-detection solution is not suitable for end-to-end autonomous driving. (4) V2X-ViT exhibits better performance than UniV2X at AMOTA (0.287 *vs* 0.239), but it requires much more transmission cost (2.56×10^6 *vs* 6.94×10^4). When we further compress the V2X-ViT transmission to a level similar to UniV2X with Where2comm, there is a significant performance drop (from 0.287 to 0.071 at AMOTA). These outcomes underscore the capability of our infrastructure agent queries and agent fusion module in enhancing agent perception ability with light transmission cost.

Online Mapping Results. We implement No Fusion, Early Fusion, and CoBEVT [51] for online mapping on DAIR-V2X. All methods are re-implemented using BEVFormer [27]. The mapping performance is reported with Segmentation Intersection over Union (IoU) (%) as the evaluation metric in Table 5. UniV2X demonstrates notable improvements in lane perception and crossing perception compared No Fusion, Early Fusion and CoBEVT, respectively. Moreover, compared with Early Fusion and CoBEVT, UniV2X requires less than 1/10th of the transmission cost. These results indicate that infrastructure lane queries and cross-view lane fusion are effective in enhancing online mapping ability.

Table 5: Online Mapping Evaluation Results.

Method	IoU-Lane (%) \uparrow	IoU-Crosswalk (%) \uparrow	Trans. Cost (BPS) \downarrow
No Fusion	6.4	2.7	0
Early Fusion	16.7	17.8	8.19×10^7
CoBEVT [51]	15.6	16.4	2.56×10^6
UniV2X (Ours)	17.8	19.8	1.47×10^5

Occupancy Prediction Results. Concerning the evaluation of occupancy prediction, as depicted in Table 6, UniV2X exhibits notably superior performance compared to No Fusion in both near and far regions. Particularly, UniV2X achieves **+5.7** and **+13.4** improvement in IoU-n (%) and IoU-f (%) respectively. Here, "IoU-n" and "IoU-f" denote evaluation ranges of $30 \times 30\text{m}$ and $50 \times 50\text{m}$, respectively. These results underscore the effectiveness of our sparse-dense hybrid transmitted data in significantly enhancing occupancy prediction.

Table 6: Occupancy Prediction Evaluation Results.

Method	IoU-n (%) \uparrow	IoU-f (%) \uparrow
No Fusion	16.3	13.1
UniV2X	22.0 (+5.7)	26.5 (+13.4)

4.3 Ablation Study

Roles of Each Fusion Module. In this part, we investigate the contributions of each fusion module within UniV2X to the enhancement of final planning performance. In evaluating the trained UniV2X, we only fuse agent queries, lane queries, and occupancy probability maps, respectively. We assess each individual fusion module and present the results in Table 7.

As evident in Table 7, AgentFusion and OccFusion exhibit an average collision rate decrease of 0.15% and 0.30%, respectively, while LaneFusion shows a marginal decrease in the average collision rate. Notably, when AgentFusion and OccFusion are combined, there is a more pronounced decrease in the collision rate. These results emphasize the effectiveness of AgentFusion and OccFusion in enhancing collision avoidance performance. However, it is crucial to note that the lack of a substantial decrease in the collision rate with LaneFusion does not imply its ineffectiveness for final planning. Metrics such as the lane violation rate [64] are essential for measuring planning output, reflecting the map enhancement for fewer collisions with lane lines and better adherence to traffic rules. In our future work, we plan to incorporate additional evaluation metrics for a more comprehensive assessment of planning performance.

Table 7: Planning Evaluation Results of UniV2X with Each Fusion Module. AgentFusion and OccFusion both play a role in reducing the collision rate.

Method	L2 Error (m) \downarrow				Col. Rate(%) \downarrow			
	2.5s	3.5s	4.5s	Avg.	2.5s	3.5s	4.5s	Avg.
No Fusion	2.58	3.37	4.36	3.44	0.15	1.04	1.48	0.89
AgentFusion	2.55	3.35	4.34	3.41	0.30	1.04	0.89	0.74 (-0.15)
LaneFusion	2.58	3.37	4.36	3.44	0.15	1.04	1.48	0.89 (-0.0)
OccFusion	2.63	3.37	4.38	3.46	0.00	0.59	1.19	0.59 (-0.30)
UniV2X	2.60	3.34	4.36	3.43	0.00	0.74	0.74	0.49 (-0.40)

Reliability in Different Communication Conditions. We evaluate UniV2X under various communication conditions. Here we assess the impact of data transmission corruption. Additionally, we assess the robustness of UniV2X across different communication bandwidths and latencies, as detailed in the Appendix. We specifically utilize agent queries and fusion to illustrate this reliability.

When assessing UniV2X, our initial step involves randomly discarding 10%, 30%, 50%, 70%, and 100% of infrastructure agent queries during transmission to simulate data corruption. Following this, the retained queries are utilized for cross-view query transmission and interaction, and the performance of agent perception, encompassing object detection and tracking, is evaluated accordingly. The evaluation results depicted in Figure 4 unveil a gradual degradation in agent perception as the data corruption ratio increases. When the data corruption ratio reaches 100%, meaning only ego-vehicle sensor data can be used, the performance of UniV2X becomes comparable to that of the No Fusion model. This decline in performance is anticipated, as data corruption diminishes the complementary information crucial for ego-vehicle autonomous driving. Moreover, it is noteworthy that even in the absence of certain data due to corruption, UniV2X can maintain a basic level of performance comparable to the No Fusion model. This underscores the reliability of our transmission and cross-view data fusion mechanism.

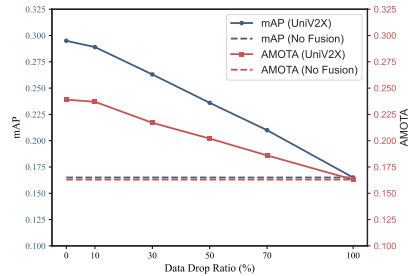


Fig. 4: Reliability on Data Corruption.

5 Conclusion

This paper presents UniV2X, a novel end-to-end framework that integrates crucial tasks from various perspectives into a single network. With a planning-oriented approach, it leverages raw sensor data while ensuring network interpretability for cooperative autonomous driving. Additionally, a sparse-dense hybrid data transmission strategy is devised to harness cross-view data and enhance overall planning performance. This transmission approach is both communication-friendly and reliable, aligning with V2X communication requirements. Empirical

results on the DAIR-V2X dataset validate the efficacy of our proposed approach.

Limitations and Future Work. The framework involves multiple modules and different agent perspectives, resulting in a high degree of complexity. As a result, several interaction fusion modules within the framework remain in preliminary stages. Further refinement is essential for optimizing the internal design of the subsequent framework. Moreover, the current planning evaluations only adopt L2 Errors and Collision Rate metrics. In the future, more comprehensive evaluation metrics will be adopted to measure the planning performance. In this work, we only consider open-loop evaluation for end-to-end autonomous driving. We will conduct more closed-loop experiments to evaluate our UniV2X.

References

1. Bodla, N., Singh, B., Chellappa, R., Davis, L.S.: Soft-nms—improving object detection with one line of code. In: Proceedings of the IEEE international conference on computer vision. pp. 5561–5569 (2017) [6](#)
2. Bojarski, M., Del Testa, D., Dworakowski, D., Firner, B., Flepp, B., Goyal, P., Jackel, L.D., Monfort, M., Muller, U., Zhang, J., et al.: End to end learning for self-driving cars. arXiv preprint arXiv:1604.07316 (2016) [4](#)
3. Caesar, H., Bankiti, V., Lang, A.H., Vora, S., Liong, V.E., Xu, Q., Krishnan, A., Pan, Y., Baldan, G., Beijbom, O.: nuscenes: A multimodal dataset for autonomous driving. In: Proceedings of the IEEE/CVF conference on computer vision and pattern recognition. pp. 11621–11631 (2020) [4](#), [11](#), [22](#), [23](#)
4. Carion, N., Massa, F., Synnaeve, G., Usunier, N., Kirillov, A., Zagoruyko, S.: End-to-end object detection with transformers. In: European conference on computer vision. pp. 213–229. Springer (2020) [6](#)
5. Chen, Q., Tang, S., Yang, Q., Fu, S.: Cooper: Cooperative perception for connected autonomous vehicles based on 3d point clouds. In: 2019 IEEE 39th International Conference on Distributed Computing Systems (ICDCS). pp. 514–524. IEEE (2019) [3](#)
6. Chen, Z., Shi, Y., Jia, J.: Transiff: An instance-level feature fusion framework for vehicle-infrastructure cooperative 3d detection with transformers. In: Proceedings of the IEEE/CVF International Conference on Computer Vision. pp. 18205–18214 (2023) [2](#), [4](#), [6](#)
7. Codevilla, F., Müller, M., López, A., Koltun, V., Dosovitskiy, A.: End-to-end driving via conditional imitation learning. In: 2018 IEEE international conference on robotics and automation (ICRA). pp. 4693–4700. IEEE (2018) [4](#)
8. Creß, C., Zimmer, W., Strand, L., Fortkord, M., Dai, S., Lakshminarasimhan, V., Knoll, A.: A9-dataset: Multi-sensor infrastructure-based dataset for mobility research. In: 2022 IEEE Intelligent Vehicles Symposium (IV). pp. 965–970. IEEE (2022) [4](#)
9. Cui, J., Qiu, H., Chen, D., Stone, P., Zhu, Y.: Coopernaut: End-to-end driving with cooperative perception for networked vehicles. In: Proceedings of the IEEE/CVF Conference on Computer Vision and Pattern Recognition. pp. 17252–17262 (2022) [2](#), [4](#), [11](#), [21](#)
10. Dong, J., Chen, Q., Qu, D., Lu, H., Ganlath, A., Yang, Q., Chen, S., Labi, S.: Lidar-based cooperative relative localization. In: 2023 IEEE Intelligent Vehicles Symposium (IV). pp. 1–8. IEEE (2023) [2](#)
11. Dosovitskiy, A., Ros, G., Codevilla, F., Lopez, A., Koltun, V.: Carla: An open urban driving simulator. In: Conference on robot learning. pp. 1–16. PMLR (2017) [20](#)

12. Fan, S., Yu, H., Yang, W., Yuan, J., Nie, Z.: Quest: Query stream for vehicle-infrastructure cooperative perception. *IEEE international conference on robotics and automation (ICRA)* (2024) [4](#), [6](#)
13. Gu, J., Zhang, J., Zhang, M., Meng, W., Xu, S., Zhang, J., Zhang, X.: Feaco: Reaching robust feature-level consensus in noisy pose conditions. In: *Proceedings of the 31st ACM International Conference on Multimedia*. pp. 3628–3636 (2023) [9](#)
14. Hao, R., Fan, S., Dai, Y., Zhang, Z., Li, C., Wang, Y., Yu, H., Yang, W., Jirui, Y., Nie, Z.: Rcooper: A real-world large-scale dataset for roadside cooperative perception. *Proceedings of the IEEE/CVF Conference on Computer Vision and Pattern Recognition* (2024) [1](#)
15. Hu, A., Murez, Z., Mohan, N., Dudas, S., Hawke, J., Badrinarayanan, V., Cipolla, R., Kendall, A.: FIERY: Future instance prediction in bird’s-eye view from surround monocular cameras (2021) [23](#)
16. Hu, Y., Yang, J., Chen, L., Li, K., Sima, C., Zhu, X., Chai, S., Du, S., Lin, T., Wang, W., et al.: Planning-oriented autonomous driving. In: *Proceedings of the IEEE/CVF Conference on Computer Vision and Pattern Recognition*. pp. 17853–17862 (2023) [3](#), [4](#), [6](#), [10](#), [11](#), [23](#)
17. Hu, Y., Fang, S., Lei, Z., Zhong, Y., Chen, S.: Where2comm: Communication-efficient collaborative perception via spatial confidence maps. *Advances in neural information processing systems* **35**, 4874–4886 (2022) [2](#), [4](#), [12](#)
18. Hu, Y., Lu, Y., Xu, R., Xie, W., Chen, S., Wang, Y.: Collaboration helps camera overtake lidar in 3d detection. In: *Proceedings of the IEEE/CVF Conference on Computer Vision and Pattern Recognition*. pp. 9243–9252 (2023) [2](#), [3](#), [12](#)
19. Jia, X., Wu, P., Chen, L., Xie, J., He, C., Yan, J., Li, H.: Think twice before driving: Towards scalable decoders for end-to-end autonomous driving. In: *Proceedings of the IEEE/CVF Conference on Computer Vision and Pattern Recognition*. pp. 21983–21994 (2023) [4](#)
20. Jiang, Y., Javanmard, E., Nakazato, J., Tsukada, M., Esaki, H.: Roadside lidar assisted cooperative localization for connected autonomous vehicles. *ACM Intelligent Computing and its Emerging Applications (ICEA)* (2023) [2](#)
21. Kendall, A., Hawke, J., Janz, D., Mazur, P., Reda, D., Allen, J.M., Lam, V.D., Bewley, A., Shah, A.: Learning to drive in a day. In: *2019 International Conference on Robotics and Automation (ICRA)*. pp. 8248–8254. *IEEE* (2019) [4](#)
22. Kuhn, H.W.: The hungarian method for the assignment problem. *Naval research logistics quarterly* **2**(1-2), 83–97 (1955) [8](#)
23. Kuhn, H.W.: The hungarian method for the assignment problem. In: *50 Years of Integer Programming* (2010) [12](#)
24. Lei, Z., Ren, S., Hu, Y., Zhang, W., Chen, S.: Latency-aware collaborative perception. In: *ECCV* (2022) [4](#)
25. Li, Y., Ma, D., An, Z., Wang, Z., Zhong, Y., Chen, S., Feng, C.: V2x-sim: Multi-agent collaborative perception dataset and benchmark for autonomous driving. *IEEE Robotics and Automation Letters* **7**(4), 10914–10921 (2022) [3](#), [4](#), [10](#), [20](#)
26. Li, Y., Ren, S., Wu, P., Chen, S., Feng, C., Zhang, W.: Learning distilled collaboration graph for multi-agent perception. *Advances in Neural Information Processing Systems* **34**, 29541–29552 (2021) [3](#), [12](#)
27. Li, Z., Wang, W., Li, H., Xie, E., Sima, C., Lu, T., Qiao, Y., Dai, J.: Bevformer: Learning bird’s-eye-view representation from multi-camera images via spatiotemporal transformers. In: *European conference on computer vision*. pp. 1–18. Springer (2022) [6](#), [12](#), [13](#)
28. Li, Z., Wang, W., Xie, E., Yu, Z., Anandkumar, A., Alvarez, J.M., Luo, P., Lu, T.: Panoptic segformer: Delving deeper into panoptic segmentation with transformers. In: *Proceedings of the IEEE/CVF Conference on Computer Vision and Pattern Recognition*. pp. 1280–1289 (2022) [6](#)

29. Li, Z., Yu, Z., Lan, S., Li, J., Kautz, J., Lu, T., Alvarez, J.M.: Is ego status all you need for open-loop end-to-end autonomous driving? In: Proceedings of the IEEE/CVF Conference on Computer Vision and Pattern Recognition (2024) **11**, **21**
30. Liang, X., Wang, T., Yang, L., Xing, E.: CirI: Controllable imitative reinforcement learning for vision-based self-driving. In: Proceedings of the European conference on computer vision (ECCV). pp. 584–599 (2018) **4**
31. Lin, C., Tian, D., Duan, X., Zhou, J., Zhao, D., Cao, D.: V2vformer: Vehicle-to-vehicle cooperative perception with spatial-channel transformer. IEEE Transactions on Intelligent Vehicles (2024) **3**
32. Lopez, P.A., Behrlich, M., Bieker-Walz, L., Erdmann, J., Flötteröd, Y.P., Hilbrich, R., Lücken, L., Rummel, J., Wagner, P., Wießner, E.: Microscopic traffic simulation using sumo. In: 2018 21st international conference on intelligent transportation systems (ITSC). pp. 2575–2582. IEEE (2018) **20**
33. Mao, R., Guo, J., Jia, Y., Sun, Y., Zhou, S., Niu, Z.: Dolphins: Dataset for collaborative perception enabled harmonious and interconnected self-driving. In: Proceedings of the Asian Conference on Computer Vision. pp. 4361–4377 (2022) **4**
34. Prakash, A., Chitta, K., Geiger, A.: Multi-modal fusion transformer for end-to-end autonomous driving. In: Proceedings of the IEEE/CVF Conference on Computer Vision and Pattern Recognition. pp. 7077–7087 (2021) **4**
35. Qiu, C., Yadav, S., Squicciarini, A., Yang, Q., Fu, S., Zhao, J., Xu, C.: Distributed data-sharing consensus in cooperative perception of autonomous vehicles. In: 2022 IEEE 42nd International Conference on Distributed Computing Systems (ICDCS). pp. 1212–1222. IEEE (2022) **2**
36. Ruan, H., Yu, H., Yang, W., Fan, S., Tang, Y., Nie, Z.: Learning cooperative trajectory representations for motion forecasting. arXiv preprint arXiv:2311.00371 (2023) **2**, **3**
37. Sadat, A., Casas, S., Ren, M., Wu, X., Dhawan, P., Urtasun, R.: Perceive, predict, and plan: Safe motion planning through interpretable semantic representations. In: Computer Vision—ECCV 2020: 16th European Conference, Glasgow, UK, August 23–28, 2020, Proceedings, Part XXIII 16. pp. 414–430. Springer (2020) **4**
38. Shao, H., Wang, L., Chen, R., Li, H., Liu, Y.: Safety-enhanced autonomous driving using interpretable sensor fusion transformer. In: Conference on Robot Learning. pp. 726–737. PMLR (2023) **4**
39. Sizhe, W., Yuxi, W., Yue, H., Yifan, L., Yiqi, Z., Siheng, C., Zhang, Y.: Asynchrony-robust collaborative perception via bird’s eye view flow. In: Thirty-seventh Conference on Neural Information Processing Systems (2023) **4**
40. Song, R., Liang, C., Cao, H., Yan, Z., Zimmer, W., Gross, M., Festag, A., Knoll, A.: Collaborative semantic occupancy prediction with hybrid feature fusion in connected automated vehicles. Proceedings of the IEEE/CVF Conference on Computer Vision and Pattern Recognition (2024) **2**
41. Tesla: Tesla AI Day. https://www.youtube.com/watch?v=ODSJsviD_SU (2022) **5**
42. Teufel, S., Gamberdinger, J., Volk, G., Bringmann, O.: Collective pv-rcnn: A novel fusion technique using collective detections for enhanced local lidar-based perception. In: 2023 IEEE 26th International Conference on Intelligent Transportation Systems (ITSC). pp. 1828–1834. IEEE (2023) **3**
43. Tian, X., Jiang, T., Yun, L., Wang, Y., Wang, Y., Zhao, H.: Occ3d: A large-scale 3d occupancy prediction benchmark for autonomous driving. arXiv preprint arXiv:2304.14365 (2023) **6**
44. Tianhang, W., Guang, C., Kai, C., Zhengfa, L., Bo, Z., Alois, K., Jiang, C.: Umc: A unified bandwidth-efficient and multi-resolution based collaborative perception framework. In: Proceedings of the IEEE/CVF International Conference on Computer Vision. pp. 23383–23392 (2023) **2**

45. Valiente, R., Zaman, M., Ozer, S., Fallah, Y.P.: Controlling steering angle for cooperative self-driving vehicles utilizing cnn and lstm-based deep networks. In: 2019 IEEE intelligent vehicles symposium (IV). pp. 2423–2428. IEEE (2019) **2**, **4**
46. Wang, T., Kim, S., Ji, W., Xie, E., Ge, C., Chen, J., Li, Z., Luo, P.: Deepaccident: A motion and accident prediction benchmark for v2x autonomous driving. arXiv preprint arXiv:2304.01168 (2023) **2**
47. Wang, T.H., Manivasagam, S., Liang, M., Yang, B., Zeng, W., Urtasun, R.: V2vnet: Vehicle-to-vehicle communication for joint perception and prediction. In: Computer Vision—ECCV 2020: 16th European Conference, Glasgow, UK, August 23–28, 2020, Proceedings, Part II 16. pp. 605–621. Springer (2020) **2**, **3**, **11**
48. Wei, Y., Zhao, L., Zheng, W., Zhu, Z., Zhou, J., Lu, J.: Surroundocc: Multi-camera 3d occupancy prediction for autonomous driving. In: Proceedings of the IEEE/CVF International Conference on Computer Vision. pp. 21729–21740 (2023) **6**
49. Weng, X., Wang, J., Held, D., Kitani, K.: Ab3dmot: A baseline for 3d multi-object tracking and new evaluation metrics. arXiv preprint arXiv:2008.08063 (2020) **12**
50. Wu, P., Jia, X., Chen, L., Yan, J., Li, H., Qiao, Y.: Trajectory-guided control prediction for end-to-end autonomous driving: A simple yet strong baseline. *Advances in Neural Information Processing Systems* **35**, 6119–6132 (2022) **4**
51. Xu, R., Tu, Z., Xiang, H., Shao, W., Zhou, B., Ma, J.: Cobevt: Cooperative bird’s eye view semantic segmentation with sparse transformers. arXiv preprint arXiv:2207.02202 (2022) **2**, **3**, **13**
52. Xu, R., Xiang, H., Tu, Z., Xia, X., Yang, M.H., Ma, J.: V2x-vit: Vehicle-to-everything cooperative perception with vision transformer. In: European conference on computer vision. pp. 107–124. Springer (2022) **4**, **12**
53. Xu, R., Xiang, H., Xia, X., Han, X., Li, J., Ma, J.: Opv2v: An open benchmark dataset and fusion pipeline for perception with vehicle-to-vehicle communication. In: 2022 International Conference on Robotics and Automation (ICRA). pp. 2583–2589. IEEE (2022) **4**
54. Yang, D., Yang, K., Wang, Y., Liu, J., Xu, Z., Yin, R., Zhai, P., Zhang, L.: How2comm: Communication-efficient and collaboration-pragmatic multi-agent perception. In: Thirty-seventh Conference on Neural Information Processing Systems (2023) **3**
55. Yang, K., Yang, D., Zhang, J., Li, M., Liu, Y., Liu, J., Wang, H., Sun, P., Song, L.: Spatio-temporal domain awareness for multi-agent collaborative perception. In: Proceedings of the IEEE/CVF International Conference on Computer Vision. pp. 23383–23392 (2023) **9**
56. Yang, K., Yang, D., Zhang, J., Wang, H., Sun, P., Song, L.: What2comm: Towards communication-efficient collaborative perception via feature decoupling. In: Proceedings of the 31st ACM International Conference on Multimedia. pp. 7686–7695 (2023) **4**
57. Yang, L., Tang, T., Li, J., Chen, P., Yuan, K., Wang, L., Huang, Y., Zhang, X., Yu, K.: Bevheight++: Toward robust visual centric 3d object detection. arXiv preprint arXiv:2309.16179 (2023) **1**
58. Yang, L., Yu, K., Tang, T., Li, J., Yuan, K., Wang, L., Zhang, X., Chen, P.: Bevheight: A robust framework for vision-based roadside 3d object detection. In: Proceedings of the IEEE/CVF Conference on Computer Vision and Pattern Recognition. pp. 21611–21620 (2023) **1**
59. Ye, X., Shu, M., Li, H., Shi, Y., Li, Y., Wang, G., Tan, X., Ding, E.: Rope3d: The roadside perception dataset for autonomous driving and monocular 3d object detection task. In: Proceedings of the IEEE/CVF Conference on Computer Vision and Pattern Recognition. pp. 21341–21350 (2022) **1**
60. Yu, H., Luo, Y., Shu, M., Huo, Y., Yang, Z., Shi, Y., Guo, Z., Li, H., Hu, X., Yuan, J., et al.: Dair-v2x: A large-scale dataset for vehicle-infrastructure cooperative

- 3d object detection. In: Proceedings of the IEEE/CVF Conference on Computer Vision and Pattern Recognition. pp. 21361–21370 (2022) [1](#), [3](#), [4](#), [5](#), [10](#), [20](#), [22](#), [24](#)
61. Yu, H., Tang, Y., Xie, E., Mao, J., Luo, P., Nie, Z.: Flow-based feature fusion for vehicle-infrastructure cooperative 3d object detection. In: Advances in Neural Information Processing Systems (NeurIPS) (2023) [2](#)
 62. Yu, H., Tang, Y., Xie, E., Mao, J., Yuan, J., Luo, P., Nie, Z.: Vehicle-infrastructure cooperative 3d object detection via feature flow prediction. arXiv preprint arXiv:2303.10552 (2023) [4](#), [7](#), [8](#), [10](#)
 63. Yu, H., Yang, W., Ruan, H., Yang, Z., Tang, Y., Gao, X., Hao, X., Shi, Y., Pan, Y., Sun, N., et al.: V2x-seq: A large-scale sequential dataset for vehicle-infrastructure cooperative perception and forecasting. In: Proceedings of the IEEE/CVF Conference on Computer Vision and Pattern Recognition. pp. 5486–5495 (2023) [1](#), [2](#), [4](#), [5](#), [7](#), [8](#), [10](#)
 64. Zeng, W., Luo, W., Suo, S., Sadat, A., Yang, B., Casas, S., Urtasun, R.: End-to-end interpretable neural motion planner. In: Proceedings of the IEEE/CVF Conference on Computer Vision and Pattern Recognition. pp. 8660–8669 (2019) [13](#)
 65. Zeng, W., Wang, S., Liao, R., Chen, Y., Yang, B., Urtasun, R.: Dsdnet: Deep structured self-driving network. In: Computer Vision–ECCV 2020: 16th European Conference, Glasgow, UK, August 23–28, 2020, Proceedings, Part XXI 16. pp. 156–172. Springer (2020) [4](#)
 66. Zhai, J.T., Feng, Z., Du, J., Mao, Y., Liu, J.J., Tan, Z., Zhang, Y., Ye, X., Wang, J.: Rethinking the open-loop evaluation of end-to-end autonomous driving in nuscenes. arXiv preprint arXiv:2305.10430 (2023) [21](#)
 67. Zhang, Y., Zhu, Z., Zheng, W., Huang, J., Huang, G., Zhou, J., Lu, J.: BEVerse: Unified perception and prediction in birds-eye-view for vision-centric autonomous driving. arXiv preprint arXiv:2205.09743 (2022) [23](#)

A Experiment Results on More Dataset

In this section, we apply UniV2X to the V2X-Sim dataset [25] to showcase its effectiveness across a broader spectrum of datasets and V2X scenarios.

V2X-Sim Dataset. The V2X-Sim dataset [25] is a synthetic dataset for cooperative autonomous driving, developed through the integration of Carla Simulator [11] and SUMO [32] co-simulation. This dataset comprises 100 scenes, and each scene contains synchronized image and point cloud sequences, at a key frame rate of 5Hz, from roadside sensors and sensors mounted on five autonomous driving vehicles. The dataset also provides a diverse array of meticulously annotated ground truths, including 3D bounding boxes and tracking IDs.

Experiment Settings and Results. We choose two autonomous vehicles from V2X-Sim and designate one as the ego vehicle to establish V2V scenes. To maintain consistency with the implementation on DAIR-V2X [60], we equip each autonomous vehicle solely with a front camera sensor. For this experiment, we utilize only one-fifth of the dataset to streamline the results. Considering the absence of evaluation metrics reflecting online mapping’s impact on planning, such as lane violation, we exclude the online mapping task from this experiment. We proceed with training and evaluation of UniV2X on V2X-Sim using settings akin to those in DAIR-V2X [60]. The experimental outcomes are detailed in Table 8, Table 9, and Table 10.

In comparison to No Fusion, our UniV2X exhibits performance improvements across various aspects, encompassing final planning (with a decrease from 2.0% to 1.75% in average Collision Rate) and all intermediate outputs, including agent perception (indicated by an increase from 7.0% to 7.6% in mAP) and occupancy prediction (with improvements from 18.9% to 19.7% in IoU-far). These experimental results underscore the effectiveness of our UniV2X across a broader spectrum of datasets and V2V scenes.

Table 8: Planning Evaluation Results on V2X-Sim Dataset [25].

Method	L2 Error (m)↓				Col. Rate (%)↓			
	0.8s	1.4s	2.0s	Avg.	0.8s	1.4s	2.0s	Avg.
No Fusion	0.98	1.79	2.65	1.81	2.0	2.25	1.75	2.0
UniV2X	0.97	1.77	2.66	1.80	1.75	2.0	1.5	1.75

Table 9: Agent Perception Evaluation Results on V2X-Sim Dataset [25].

method	mAP (%)↑	AMOTA (%)↑
No Fusion	7.0	0.6
UniV2X	7.6	1.7

Table 10: Occupancy Evaluation Results on V2X-Sim Dataset [25].

method	IoU-n (%)↑	IoU-f (%)↑
No Fusion	15.9	18.9
UniV2X	16.1	19.7

B Ego Status in Planning Performance.

The significance of ego status, particularly its velocity, has been emphasized in discussions on open-loop end-to-end autonomous driving. Velocity aids in plan-

ning trajectories akin to those of expert drivers, thereby substantially mitigating L2 Error [29, 66]. In this section, we delve into the impact of ego-vehicle velocity.

Experiment Settings. We conduct two additional experiments:

- CooperNaut [9] with ego-vehicle velocity: In this experiment, we incorporate ego-vehicle velocity into an 8-dimensional feature and concatenate it with the fused Bird’s Eye View (BEV) feature. The resulting concatenated feature is then passed through a Multi-Layer Perceptron (MLP) to generate the final planning path. We subsequently train this model using the same configuration as the CooperNaut baseline, denoting it as "CooperNaut+V".
- UniV2X with ego-vehicle velocity: In this experiment, we integrate velocity information into an 8-dimensional feature vector, which is then concatenated with the ego planning query. We then train this model under the same conditions as UniV2X, naming it "UniV2X+V".

Experiment Results. As illustrated in Table 11, our UniV2X model, when augmented with embedded ego-vehicle velocity, demonstrates reductions of 1.94 meters and 0.24% in average L2 error and average collision rate, respectively. Similarly, CooperNaut with ego-vehicle velocity exhibits decreases of 3.36 meters and 0.98% in average L2 error and average collision rate, respectively. In summary, UniV2X achieves superior collision rate results compared to both CooperNaut and CooperNaut+V, reaching state-of-the-art (SOTA) performance in collision rate, regardless of whether ego-vehicle velocity is considered. However, it’s crucial to acknowledge that integrating ego-vehicle velocity into the model may introduce bias, as velocity encapsulates historical information about the ego-vehicle. This inclusion may inadvertently transform the planning problem into one of ego-vehicle trajectory prediction, potentially skewing overall evaluation results. This consideration aligns with research discussed in [29, 66].

Table 11: More Planning Evaluation Results Considering Ego-Vehicle Velocity.

Method	L2 (m)↓				Col. Rate (%)↓				Trans. Cost↓
	2.5s	3.5s	4.5s	Avg.	2.5s	3.5s	4.5s	Avg.	
CooperNaut [9]	3.83	5.26	6.69	5.26	0.59	1.92	1.63	1.38	8.19×10^7
CooperNaut+V [9]	1.55	1.90	2.26	1.90	0.15	0.15	0.89	0.40	8.19×10^7
UniV2X	2.60	3.34	4.36	3.43	0.00	0.74	0.74	0.49	8.09×10^5
UniV2X+V	1.35	1.41	1.71	1.49	0.00	0.15	0.59	0.25	8.09×10^5

C Flow Prediction for Latency Compensation

In this section, we explore how our flow prediction can mitigate communication latency. Specifically, we employ Agent Perception to demonstrate this effect.

Experiment Settings. We evaluate UniV2X under two distinct latency conditions: $0ms$ and $500ms$. Additionally, to examine the influence of latency on UniV2X’s performance, we excluded the prediction module from UniV2X. This version is denoted as UniV2X (without prediction), abbreviated as "UniV2X-O", and was evaluated under both $0ms$ and $500ms$ latency settings.

Experiment Results. As shown in Table 12, UniV2X-O has a notable decline in perception performance under 500ms latency (a decrease of 3.6% in mAP and 1.2% in AMOTA compared to scenarios with no latency). However, with the inclusion of flow prediction, UniV2X demonstrates minimal performance degradation under 500ms latency (only a decrease of 1.2% in mAP and 0.4% in AMOTA). These results demonstrate that latency can impact fusion performance and our feature prediction module can mitigate this performance decline.

Table 12: Agent Perception Evaluation Results with Latency.

Method	Latency (ms)	mAP (%) ↑	AMOTA (%) ↑
UniV2X-O	0	29.5	23.9
UniV2X-O	500	25.9 (-3.6)	22.7 (-1.2)
UniV2X	0	29.5	23.9
UniV2X	500	28.5 (-1.0)	23.5 (-0.4)

D Different Communication Bandwidth Constraints

In this section, we investigate UniV2X’s adaptability to varying communication bandwidths. Specifically, we impose different bandwidth constraints on UniV2X transmission while maximizing the retention of queries and probability maps based on data scores. We present UniV2X’s performance across different communication bandwidths in Table 13. Across configurations ranging from 0 Mb/s to 1 Mb/s, UniV2X consistently enhances autonomous driving performance, including planning and intermediate outputs. This highlights its ability to adapt to diverse communication bandwidth constraints.

Table 13: Different Communication Bandwidth Configurations.

Bandwidth (Mb/s)	0.0	0.3	0.5	0.7	1.0
Perception: mAP (%)	16.5	21.0	23.6	26.3	29.5
Mapping: Lane (%)	6.4	10.9	13.2	15.0	17.7
Occ: IoU-f. (%)	13.1	20.4	23.1	25.0	26.5
Planning: Col. Rate (%)	1.48	1.04	1.04	0.74	0.74

E Evaluation Metrics

In this section, we detail the evaluation metrics used to assess the agent perception, online mapping, occupancy prediction, planning, and transmission cost.

Object Detection. We evaluate the detection performance using the mean Average Precision (mAP) metric, which is commonly used in previous works such as [3, 60]. The AP is calculated based on the 11-points interpolated precision-recall curve and is defined as follows:

$$AP = \frac{1}{11} \sum_{r \in \{0.0, \dots, 1.0\}} AP_r = \frac{1}{11} \sum_{r \in \{0.0, \dots, 1.0\}} P_{interp}(r), \quad (6)$$

where $P_{interp}(r) = \max_{\tilde{r} \geq r} p(\tilde{r})$, and a prediction is considered positive if the Intersection over Union (IoU) is greater than or equal to 0.5. We calculate the AP

for each class and then average them to obtain the mAP. In this paper, we only calculate and report Car class.

Multi-object Tracking. AMOTA and AMOTP, commonly 3D tracking evaluation metrics [3], are used to measure the performance of multi-object tracking.

Online Mapping. We categorize the online mapping tasks into two classes: lanes and crosswalks. For each class, we compute the Intersection over Union (IoU) metric, measuring the overlap between the prediction outputs and the ground truths.

Occupancy Prediction. In line with UniAD [16], we assess the accuracy of predicted occupancy using a methodology similar to that outlined in [15, 67]. Specifically, the Intersection over Union (IoU) metric quantifies categorical segmentations of the entire scene in an instance-agnostic manner. This metric is computed within Bird’s Eye View (BEV) ranges, with evaluations conducted for both near ($30\text{m}\times 30\text{m}$) and far ($50\text{m}\times 50\text{m}$) distances.

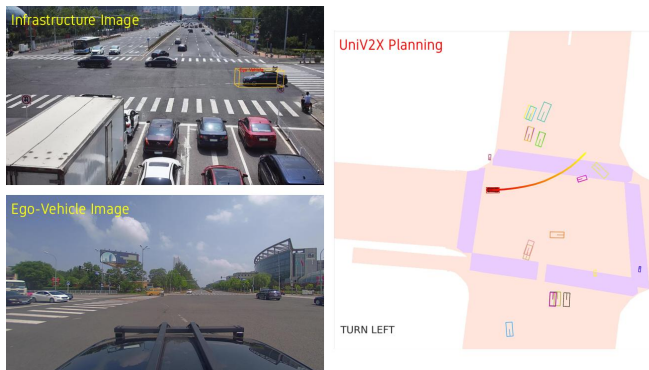
Planning. We utilize the L2 error and collision rate metrics at different timestamps to assess the planning performance. We recognize the significance of considering the lane violation rate as an additional metric for measuring planning performance, and we plan to incorporate this metric in our future evaluations.

Transmission Cost. BPS: Byte Per Second (BPS) quantifies the volume of data transmitted from the infrastructure to the ego vehicle per second, accounting for the transmission frequency. In our implementation, a transmission frequency of 2Hz is considered, and we exclude the transmission cost of calibration files and timestamps. For each transmission, the average transmission cost, denoted as \mathcal{AB} , is computed. We detail the calculation of the transmission cost for each of the two transmission forms:

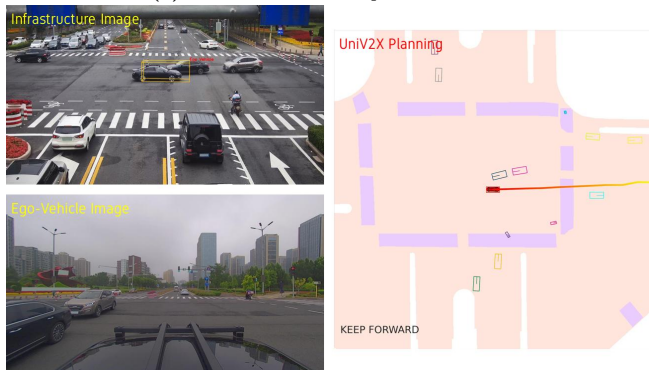
- Transmitting Queries: Each query is represented as 256-dimensional features in 32-bit float format. Consequently, each query requires eight 256×32 -bit floats, equivalent to 1024 Bytes. If ten queries are transmitted per transmission, the \mathcal{AB} of the transmission cost is 1.0×10^3 Bytes. If the transmission frequency is 2Hz, the BPS is 2.0×10^3 Bytes Per Second.
- Transmitting Features: Each feature is represented as a tensor. If the size of the feature is (24, 36, 36), and each element is encoded as a 32-bit float, the transmission cost is $24\times 36\times 36\times 4$ Bytes, amounting to 1.2×10^5 Bytes. If the transmission frequency is 2Hz, the BPS is 2.4×10^5 Bytes Per Second.

F Qualitative Visualization

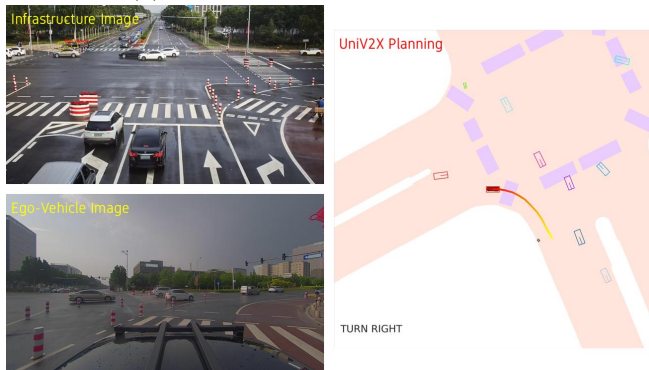
In this section, we present visualization examples to demonstrate the efficacy of UniV2X in final planning. The visualization results showcase UniV2X’s capability to address diverse driving scenarios, encompassing left turns, straight-ahead navigation, and right turns, as depicted in Figure 5.



(a) Visualization Example: Turn Left.



(b) Visualization Example: Keep Forward.



(c) Visualization Example: Turn Right.

Fig. 5: Planning Visualization of UniV2X on DAIR-V2X [60]. UniV2X consistently demonstrates the ability to generate high-quality planning outputs for diverse driving scenarios, including left turns, straight keeping, and right turns.